PERFORMANCE OPTIMISATION OF SOLAR RECEIVERS THAT USE OIL AS A HEAT TRANSFER FLUID.

JSP Mlatho[1], M McPherson[2].

[1]Physics Department, Chancellor College, University of Malawi, P.O. Box 280, Zomba, Malawi.

[2]Faculty of Applied Sciences, Cape Peninsula University of Technology, PO Box 652, Cape Town, 8000, South Africa.

Abstract

This article presents the use of a wire mesh in optimising the performance of two volumetric solar receivers that use oil as a heat transfer fluid. Computational fluid dynamics models have been used to optimise the receivers. Varies parameters (including the use of a wire mesh) of the receiver models were changed in the optimisation process. Based on the models, prototype receivers were developed and tested. After that, the models were validated against experiments and the results compare well. The results indicate that the use of a wire mesh placed inside a receiver improves its performance. An optimal wire mesh porosity was found as ≈ 0.95 mainly because the efficiency is increased without inducing an adverse pressure drop inside the receiver.

Key words

Solar receiver model, computational fluid dynamics, wire mesh, porosity, efficiency.

1. Introduction

Solar receivers are used to capture and convert solar radiation into thermal energy for storage. The stored thermal energy can be used for indirect cooking that can be carried out at a controlled rate (Mawire et al., 2009). Such solar receivers need to be optimally designed. The energy effectiveness of these solar receivers is often investigated either by experiments or through modelling (Comakli et al., 1996). In modelling, various models are run until an optimal efficiency is attained. In this work, we have designed, modelled and tested two volumetric solar receivers. The use of a wire mesh in improving the performance of the receivers has been explored using computational fluid dynamics (CFD).

In order to optimise solar receivers, modelling studies have been carried out by other authors (Kribus et al., 1998; Pitz-Paal et al., 1997). CFD was used (Meier et al., 1996) in the design and optimisation of a high temperature solar chemical reactor. It was shown in this work that CFD can be used for calculating the velocity, temperature and pressure fields as well as particle trajectories in the reactor. Pitz-Paal et al. (1997) developed a quasi 3D analytical model in order to improve the understanding of momentum and heat transfer in volumetric absorber structures. They observed that non-homogenous irradiation of the absorber in the receiver has a stronger impact on temperature distribution and efficiency. Other studies have also shown that CFD models of solar receivers can be used to optimise the performance of the receivers (Kribus et al., 1998; Reddy and Satyanarayana, 2008).

The reviewed literature shows that most of the work done on volumetric solar receivers involves the use of air or other forms of gases as the heat transfer fluid (HTF). It is for this reason that in this work two volumetric receivers, that use liquid as the HTF, were designed and their performance optimised by using a wire mesh. Firstly, CFD models of the receivers were built and effects of a wire mesh inside the receivers were tested using the models. Based on the model results, two prototype volumetric solar receivers were built and tested experimentally. The model results were then validated against the experimental results. The two receivers were developed and built for use with an SK-14 parabolic dish reflector (PDR) (Mlatho et al., 2010) in order to charge a thermal energy storage (TES) system (Mawire et al., 2009) to be used in an indirect solar cooker being designed by our group (Mlatho et al., 2010; Mawire et al., 2009).

2. The CFD models and prototype receivers.

[1]Corresponding author: Email address: stanmlatho@gmail.com, Tel: +265 881762788, Fax: +265 1524046

The particular shapes of the receiver models and the surface shapes of their apertures were chosen based on the results of a ray tracing-program of an SK-14 PDR. The models were also based on the results of the spatial extent of the focal point (FP) of the SK-14 PDR obtained with the radiometer method (Mlatho et al., 2010) that gave an aperture diameter of 0.1 m in order to obtain maximum flux concentration. This is because the energy from the receivers is intended to be delivered at high temperatures of around 200 ^{o}C. As previously stated, the prototype receivers were built based on the models.

Fig. 1 shows schematic diagrams of the CFD models of the two receivers. The first receiver termed volumetric flask (VF) receiver is designed on the basis that a parabolic surface is suitable for capturing the concentrated solar radiation (CSR) at the focal point of the SK-14 PDR as found by Mlatho et al. (2010). The model is a laboratory glass flask as shown in part (a) of Fig. 1. The reflecting plate of the VF receiver model is made of aluminium and only covers the upper-half of the round part of the flask. The round lower-half of the flask forms a curved aperture.

The second receiver is termed a volumetric box (VB) receiver as it was designed on the premise of a cylindrical cavity with a flat aperture and is also based on the results of Mlatho et al. (2010). Part (b) of Fig. 1 shows the VB receiver model made up of a metal cylinder that is closed on one end. The other end is closed with a Duran glass plate and acts as the aperture. For both receivers, the CSR is incident onto the aperture. The oil flows in and out of the receivers through the fluid inlets and outlets.

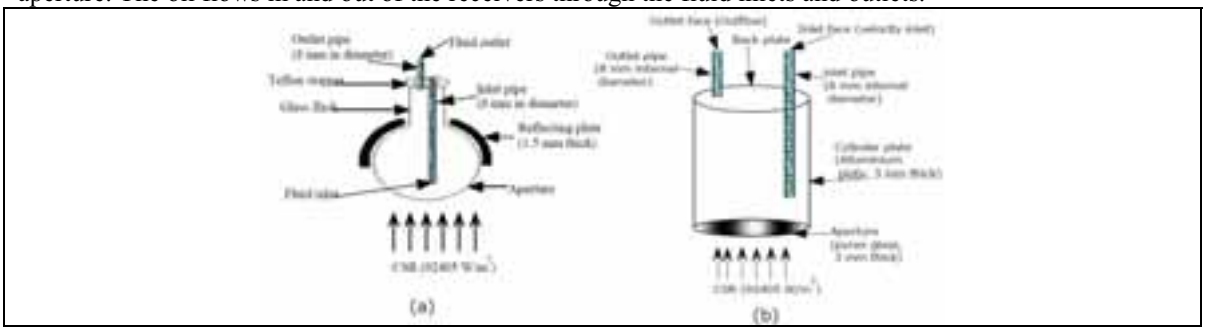

Fig. 1: The schematic diagram of the VF (a) and VB (b) receiver models.

The first prototype is a VF receiver shown in photograph (a) of Fig. 2. The glass flask is covered with galvanised steel on the top half of the round part such that the round bottom is a curved aperture of 0.1 m diameter. The second prototype is a VB receiver with a flat aperture of 0.1 m diameter (plot (b) of Fig. 2). Both apertures are made of Duran glass of the same thickness.

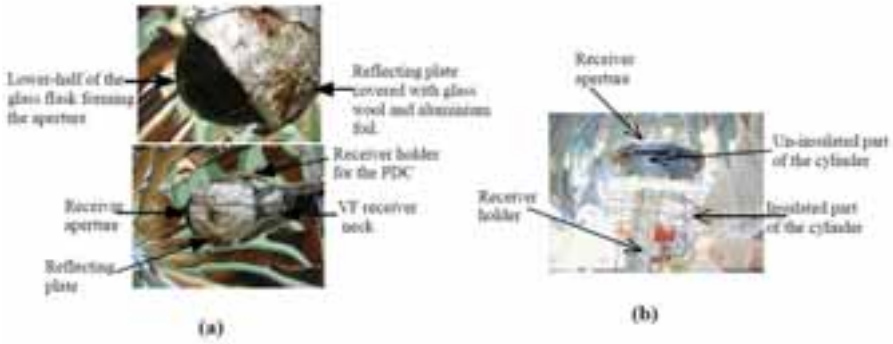

Fig. 2: Photographs of the VF receiver (a) and the VB receiver (b) showing their parts.

3. Modelling and Experimental Techniques

The CFD models were implemented for various scenarios, including the use of the wire mesh inside the receivers, in order to obtain the most suitable parameters. These were then used to build the prototypes prior to testing using various experimental techniques.

3.1 Modelling techniques

In the modelling techniques, the first step was to create and mesh the 3D models of the receivers in Gambit software. After the geometries were drawn, they were exported to Fluent software in which all the simulations were carried out. The model settings in Fluent involve a solver that is pressure-based and that

uses implicit formulation. The energy model was selected for the receiver models. The radiation model used is the Discrete ordinates model.

The oil used as the HTF in modelling and in experiments is Shell Thermia B oil (Shell, 2007). The optical properties of the oil are not available from the reviewed literature and were thus estimated from known optical properties of other oils. The oil was assumed to have a scattering coefficient of 0.002 m^{-1}, a refractive index of 1.45 and a light absorption coefficient of α = 2800 m^{-1}. We also carried out simulations using α = 600 m^{-1}, an α-value equal to that of castor oil at a wavelength of 3.5 μm (Souza, 2006). The properties of the materials used in the models are those of the materials used to build the prototype receivers.

Several boundary conditions (BCs) were implemented in the modelling. The CSR that was set at the aperture of the receiver was calculated based on the SE of the FP of the SK-14 PDR (Mlatho et al., 2010). An intercept factor of 0.5 was assumed for the receivers and this gave a CSR of 92.406 kW/m^2. This value is comparable to 100 kW/m^2, a CSR value as measured before by use of a radiometer (Mlatho et al., 2010). The glass apertures were assumed to be exposed to ambient air (T_{amb}) at a temperature of 300 K, to have an emissivity of 0.80 and a heat transfer coefficient of 15. The BC for the inlets is *velocity inlet* while that for the outlets is *outflow*.

For the VF receiver model, the upper part of the flask and its neck were set as transparent walls of thickness 1.0 mm exposed to T_{amb} = 300 K. The heat transfer coefficient was set at 10 and the emissivity at 0.8. On the outer wall of the flask is a reflecting aluminium plate that is exposed to ambient air at T_{amb} = 300 K, that has a heat transfer coefficient of 10 and an emissivity of 0.8. This outer wall has α = 0.2.

For the VB receiver model, the aluminium cylinder has an opaque wall which is exposed to ambient air at T_{amb} = 300 K, has an emissivity of 0.8 and α = 0.2. Further, it is assumed not to be properly insulated and hence has a convective heat transfer coefficient of 5.

Flow and pressure-velocity coupling models

A Laminar model was used for the oil flow in the receiver models and this is because of the low Reynolds number expected. The S-A model was also used and the results were compared with those of the Laminar model and it was found that there was a very small difference between the two. For this reason, the Laminar model was used in this work. Other turbulence models available in Fluent were also attempted but were observed not to converge and hence were abandoned.

A SIMPLE approach was employed for the pressure-velocity coupling. The momentum equations were discretized using a second order upwind scheme option. The steady-state velocity field was obtained for these models. The receiver models were run until they converged.

3.2 Experimental Techniques

In order to test the prototypes, an experimental setup was arranged that consisted of a series arrangement of a heat exchanger system, an oil reservoir, two identical positive displacement pumps, the receiver and an SK-14 PDR. Fig. 3 shows the experimental setup. The dimensions of the prototype receivers were equal to those of the receiver models. In the setup, oil from the reservoir was pumped through the receiver to the heat exchanger and back to the reservoir. The heat exchanger was used to cool the heated oil from the receiver before it flowed back to the reservoir. The reason for this is for control of the temperature of the oil in the reservoir. As a result, it was possible to restrict the temperature of the oil flowing to the receiver to ambient values.

In order to determine the efficiency of the receivers, the pumps were calibrated to displace an oil volume of ≈ 6.8 ± 0.1 ml per revolution (rev) at a zero differential pressure (ΔP) across the pump. Pump P2 was used to drive the oil through the receiver and to make the differential pressure across pump P1 to be zero. In this way, pump P1 was used as a flowmeter by counting the number of revolutions per second (rev/s) it made using a debounce switch that was connected to a totaliser channel of an Agilent data logger. The data logger was connected to a computer through an RS 232 cable. The volume flow rate of the pump is obtained from the product of rev/s and volume per revolution (vol/rev) obtained during calibration of the pumps.

Each receiver was placed at the FP of the PDR and the PDR was placed to face towards the sun such that the rays of the DSR were perpendicular to its aperture. In this way, the PDR was able to reflect the DSR to its FP. The DSR was measured by means of a Normal Incidence Pyrheliometer (NIP) which was attached to a

sun tracker. The output of the NIP was connected to the A/D converter channel of the Agilent data logger. During testing of each receiver, the inlet oil temperature (T_{in}) and the outlet oil temperature (T_{out}), together with several other receiver temperatures, were measured by using K-type thermocouples which were also connected to the data logger.

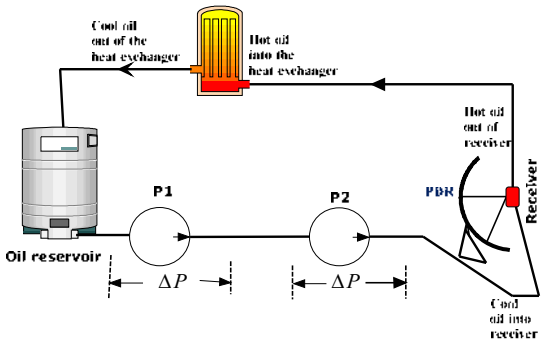

Fig. 3: An experimental setup showing the configuration of the two positive displacement pumps, P1 and P2.

The efficiency, η_1 of the receiver for converting the CSR into heat energy of the oil was calculated (Hasuike, 2006) as

$$\eta_1 = Q_{\text{useful}} \Big/ P_{\text{incident}} \qquad \text{(eq.1)}$$

where Q_{useful} is the heat per unit time gained by the oil while it is inside the receiver and P_{incident} is the input solar power (in the form of CSR). Q_{useful} is given as

$$Q_{\text{useful}} = \dot{m} c_{\text{p}} \left(T_{\text{out}} - T_{\text{in}} \right) \qquad \text{(eq.2)}$$

and P_{incident} is given as

$$P_{\text{incident}} = A_{\text{pdr}} I_{\text{b}} \qquad \text{(eq.3)}$$

where $\dot{m}$ is the mass flow rate of the oil, c_{p} is the specific heat capacity of the oil at temperature T_{rec}, A_{pdr} is the effective aperture area of the PDR (≈ 1.5 m^2) and I_{b} is the DSR. Here, T_{rec} is given as

$$T_{\text{rec}} = \left(T_{\text{in}} + T_{\text{out}} \right) \Big/ 2 \qquad \text{(eq.4)}$$

and is the temperature of the receiver.

All the variables used in the calculation of the efficiencies were measured when the receivers reached a steady state. This steady state was considered to have been reached when the receiver temperatures and the volume flow rate of the oil were no longer changing significantly. The efficiency was also measured when a wire mesh was inserted into the receivers. The porosity of the wire mesh is ≈ 0.90. The wire mesh used in the experiment is a stainless steel pot scourer that was spray-painted with black mat paint.

4. Results and discussion.

The results are presented in two sections, those obtained from the modelling process followed by those obtained from the experiments.

4.1 Modelling process

Three different efficiency values were computed for the receiver models. These are the efficiency to convert the total incident CSR into heat (η_1), the efficiency to transmit the incident CSR through the aperture (η_2), and the efficiency to convert the transmitted CSR into heat (η_3). These values were calculated for various oil velocities at the fluid inlet and are presented here in terms of the volume flow rates.

The efficiency η_1 was calculated using Eq. (1) where, in this case, Q_{useful} is the net heat transfer rate between the fluid outlet and the fluid inlet of the receiver and this can be expressed as

$$Q_{\text{useful}} = \dot{m}c_{\text{p}}T_{\text{out}} - \dot{m}c_{\text{p}}T_{\text{in}} = P_{\text{out}} - P_{\text{in}} \qquad \text{(eq.5)}$$

where P_{out} and P_{in} are the heat transfer rates at the outlet and inlet of the receiver, respectively. In this case, P_{incident} is a product of the incident CSR and the aperture area, and is constant at 730 W.

The efficiency, η_2 was calculated from a ratio of the radiation transfer rate at the aperture and P_{incident} set at the aperture. If P_{trans} is the radiation transfer rate, then

$$\eta_2 = P_{\text{trans}} \Big/ P_{\text{incident}} \qquad \text{(eq.6)}$$

while the efficiency η_3, is a ratio of Q_{useful} to P_{trans}. It is defined by

$$\eta_3 = Q_{\text{useful}} \Big/ P_{\text{trans}} \qquad \text{(eq.7)}$$

and measures how the CSR transmitted through the aperture is converted to heat.

Plots (a) and (b) of Fig. 4 show a variation of the outlet temperature (T_{out}), the mean temperature (T_{mean}) and the maximum temperature (T_{max}) of the oil with flow rate. In all cases T_{mean} is higher than T_{out}. This is because the temperature of the oil in the receivers is not uniform and is observed to be higher at the apertures than close to the fluid outlets. Thus, the aperture presents a region where the oil may attain temperatures that are higher than the allowed maximum and this can lead to a degradation of the oil. The modelled T_{max} is too high for all flow rates and may not be achieved in practice due to cooling of the apertures by the environment.

In plots (c) and (d) of the figure we show that all three efficiencies (η_1, η_2, η_3) increase with an increase in the flow rate. The highest increase is recorded for η_3 and this is mainly due to reduced heat losses (through re-radiation) and increased mass transfer rates at high volume flow rates.

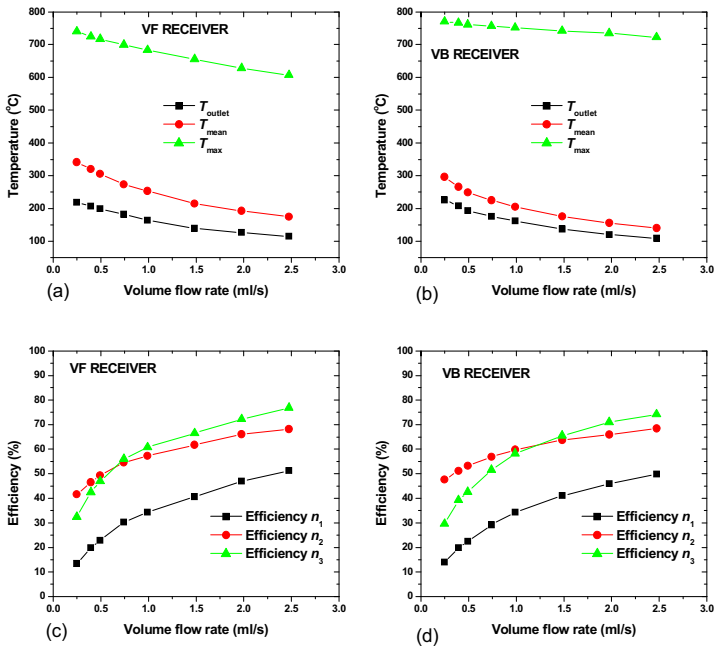

Fig. 4: Plots of the temperatures (a) and (b) and efficiencies (c) and (d) against flow rate for the two receivers with oil of α = 2800 m^{-1} and T_{in} = 26.85 °C.

The optimum flow rate occurs when $\eta_2 = \eta_3$. In plot (c) for the VF receiver, this optimum flow rate is ≈ 0.66 ml/s when η_1 is ≈ 28 % and the corresponding T_{out} is 184 °C. For the VB receiver in plot (d), the optimum flow rate is ≈ 1.25 ml/s with η_1 ≈ 38 % and T_{out} ≈ 150 °C. For flow rates that are less than the

optimum flow rate $\eta_2 > \eta_3$ while for those that are greater than the optimum flow rate the opposite holds. Thus, the receiver must be operated with a flow rate that is less than the optimum flow rate since in this situation there would be a higher amount of CSR transmitted through the aperture. In this way, the CSR available for conversion to heat in the receiver would be increased such that the overall performance of the receiver would improve.

Four sensitivity analyses were carried out on the receiver models and these are the sensitivity to the effects of α of the oil, the sensitivity to the effects of the wire mesh, the sensitivity to changes in φ of the wire mesh and the sensitivity to changes in α of the oil when $\varphi = 0.75$ for the wire mesh.

The α of oil contained in a receiver changes as the oil degrades. The degradation is partly caused by localised high temperatures (hot spots) within the receiver or by adding impurities to the oil. For this reason, the models were also run for cases when the oil had $\alpha = 600$ m^{-1}. Fig. 5 shows a variation of T_{out}, T_{mean} and T_{max} of the oil with the two α-values for the two receivers. T_{max} for $\alpha = 2800$ m^{-1} is higher than for $\alpha = 600$ m^{-1}. The high α-value results in a higher amount of CSR being absorbed by oil located close to the aperture. This leads to high temperatures at the apertures. Thus, an increase in the absorption coefficient of the oil can result in increased re-radiation losses at the aperture.

Oil of $\alpha = 600$ m^{-1} has a higher T_{out} than that of $\alpha = 2800$ m^{-1} and the difference increases with a fall in the flow rate. The same trend is observed for T_{mean}. These results imply that the easier it is for the CSR to travel through the oil (due to a low α) the higher the absorbance. The higher absorbance helps to also reduce the temperature of the oil situated at the aperture. As a result, heat losses through re-radiation are minimised. The other possibility could be that if the incident CSR that travels through the oil and is eventually absorbed by the receiver walls is high, then T_{out} and T_{mean} will be large. This also leads to the contention that if more absorption occurs at the receiver walls and away from the aperture, then T_{out} and T_{mean} will be large. Once the CSR is converted to heat at the receiver walls, it is transferred to the oil. This transfer can be enhanced by inserting a wire mesh in the receiver cavity that would increase the fluid-solid interface area.

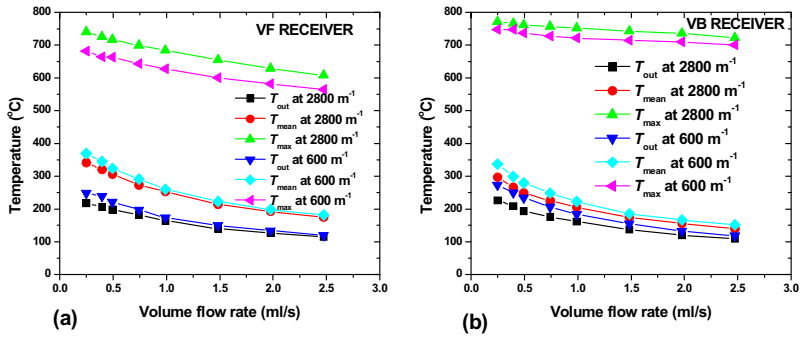

Fig. 5: A variation of oil temperatures in the VF (a) and VB (b) receivers with flow rate for oil with $\alpha = 2800$ m^{-1} and $\alpha = 600$ m^{-1}.

Fig. 6 shows the efficiencies of the receivers for the two values of α. In plot (a) and (c) respectively, η_2 for oil of $\alpha = 600$ m^{-1} is greater than η_2 for oil of $\alpha = 2800$ m^{-1}. This shows that the lower α is; the higher η_2 is and the difference increases with an increase in the flow rate. However, the two efficiencies of η_3 obtained with oil of different absorption coefficients show no remarkable difference. This implies that the absorption coefficient of the oil has little effect on η_3. The optimum flow rates (where $\eta_2 = \eta_3$), for the two receivers, are observed to move from low values to high values with a decrease in α of the oil. This is mainly because a decrease in α results in a large increase of η_2 than of η_3. However, the combined effect of η_3 and η_2, as shown through η_1 in plots (b) and (d), indicates that it increases with a decrease in the absorption coefficient of the oil. The implication, in this case, is that a decrease in the absorption coefficient increases the overall efficiency of the receiver.

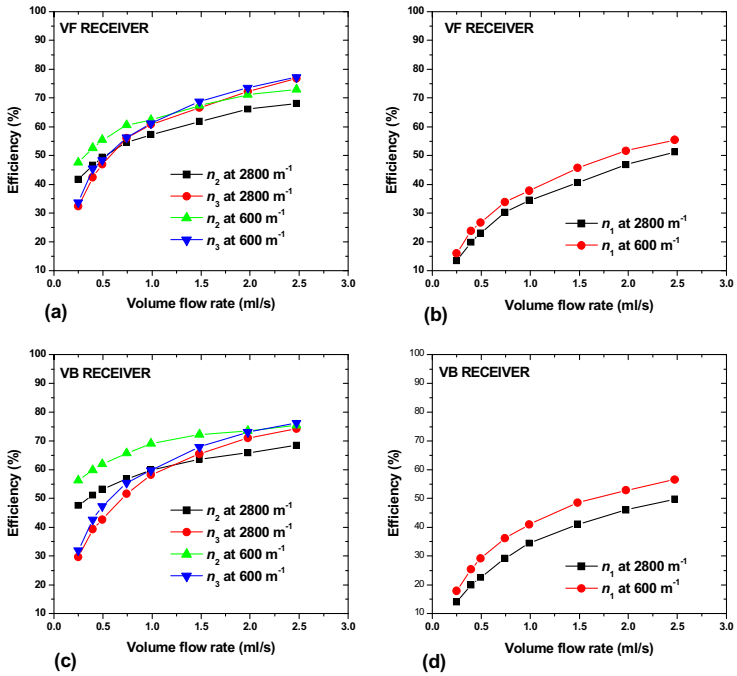

Fig. 6: A comparison of the efficiencies for the two receivers containing oil with $\alpha = 2800$ m^{-1} and $\alpha = 600$ m^{-1}.

A wire mesh was included in the model by changing the oil zone to a porous media. This was done in order to improve the mixing of the oil in the receiver and to increase the fluid-solid interface area. The porosity (φ) of the oil zone was set to 0.75. A $\varphi = 0.75$ implies that 75 % of the receiver volume is occupied by oil and 25 % is occupied by the wire mesh. If $\varphi = 1.0$ then the receiver contains oil only. The oil had $\alpha = 2800$ m^{-1} and T_{in} was 26.85 ^{o}C.

Fig. 7 shows the variation of oil temperatures when $\varphi = 1.0$ and when $\varphi = 0.75$. T_{max} for $\varphi = 0.75$ are much lower than those for $\varphi = 1.0$. For each receiver, T_{max} for $\varphi = 0.75$ is closely comparable to the corresponding T_{out} and T_{mean} for all volume flow rates. This indicates that the wire mesh improves the mixing of the oil and the distribution of the heat within the receiver. The mixing and distribution reduces the oil temperatures at the aperture and hence reduces heat losses through re-radiation. T_{out} and T_{mean} for $\varphi = 0.75$ are almost equal for all volume flow rates and are both larger than T_{out} and T_{mean} for $\varphi = 1.0$. This indicates an improvement in the performance of the receiver when it contains a wire mesh.

Fig. 8 shows a variation of the efficiencies for $\varphi = 1.0$ and $\varphi = 0.75$. In plots (a) and (c) of Fig. 8, the efficiency η_2 for $\varphi = 0.75$ is larger than that for $\varphi = 1.0$ for all flow rates. This implies that the inclusion of a wire mesh in the receiver improves the transmission of the CSR through the aperture. The reason for this is that the wire mesh reduces the temperatures at the aperture and this reduces re-radiation. A reduction in the re-radiation results in more of the incident CSR passing through the aperture. The plots also show that the efficiencies η_3 for $\varphi = 0.75$ are larger than those for $\varphi = 1.0$. For each receiver, the two efficiencies of η_3 for the different φ values are comparable for low flow rates. This is because at high flow rates, the wire mesh increases the mixing of the oil (or turbulence) in the receiver, it has a large effective thermal conductivity and it also increases the fluid-solid interface surface area onto which the oil is heated. This results in an increased efficiency η_3. The only disadvantage of using the wire mesh is an increased pressure drop within the receiver, which in turn increases the cost of pumping work (Reddy and Satyanarayana, 2008).

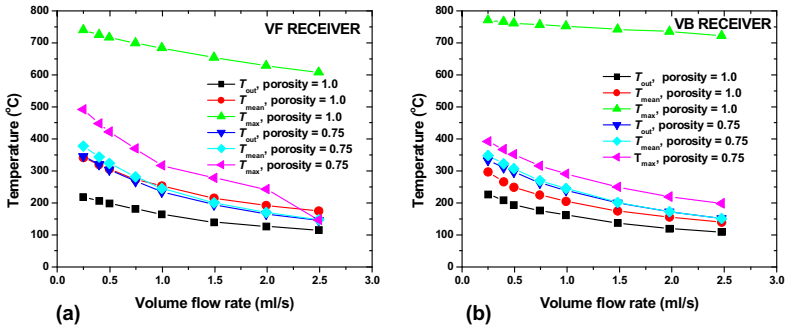

Fig. 7: Plots of oil temperatures when the two receivers have no wire mesh ($\varphi = 1.0$) and when they have a wire mesh ($\varphi = 0.75$).

High optimum flow rates are observed for $\varphi = 0.75$ than for $\varphi = 1.0$. This is mainly due to the higher η_2 recorded for $\varphi = 0.75$ than for $\varphi = 1.0$. The high optimum flow rate for a receiver containing a wire mesh signifies that the receiver will perform well than when it does not have the wire mesh. The combined effect of the wire mesh on the efficiencies η_2 and η_3 is again shown through η_1 in plots (b) and (d) of Fig. 8. The efficiency η_1 is high for $\varphi = 0.75$ than for $\varphi = 1.0$. This implies that the wire mesh does indeed improve the overall efficiency of the receivers with a pressure drop as a draw back.

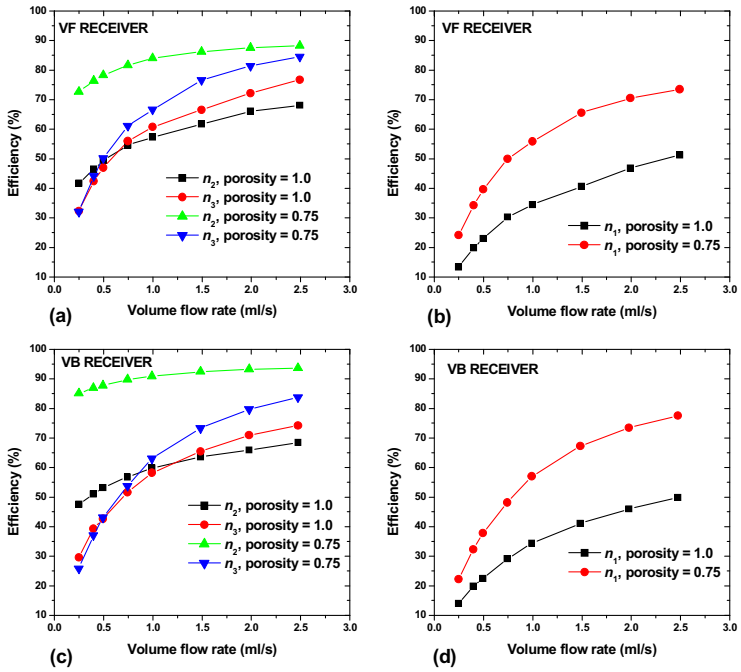

Fig. 8: A comparison of efficiencies when the receivers have no wire mesh and when they have a wire mesh.

Changes in the φ-value of the oil/mesh zone were incorporated into the models so as to test the effect of varying the density of the wire mesh. This was done for a constant flow rate of 0.99 ml/s at the fluid inlet. Plots (a) and (c) of Fig. 9 show the variation of the oil temperatures with φ. A big change in the temperatures is observed from $\varphi = 1.0$ to $\varphi = 0.95$. These deviations show the strong influence of the wire mesh on these temperatures. There is a substantial decrease of T_{max} when φ decreases from 0.95 to 0.75 for the VB receiver than for the VF receiver. This could largely be because the VF receiver is mainly composed of glass while the VB receiver is mainly composed of aluminium. However for the two receivers, there is no significant change in T_{mean} and T_{out} as φ varies from 0.95 to 0.75.

The variations of the efficiencies of the receivers with φ are shown in plots (b) and (d) of Fig. 9. A big change in each efficiency is observed when φ changes from 1.0 to 0.95. There is however no substantial change in the efficiencies when φ changes from 0.95 (less wire mesh) to 0.75 (more wire mesh).

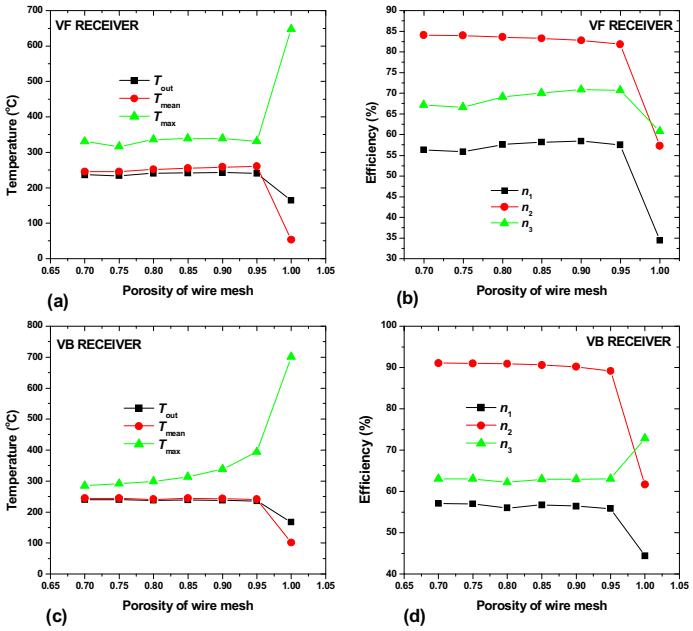

Fig. 9: The plots of the temperatures (a) and (c) and efficiencies (b) and (d) against φ when the flow rate is 0.99 ml/s and T_{in} = 26.85 °C.

The variation of the temperatures and efficiencies of the receivers show that changes in φ do not change the performance of the receivers very much. This implies that if a wire mesh is to be used in the receivers; its porosity should be close to 0.90 so as to reduce the pressure drop within the receiver.

Variations in the α-value for $\varphi = 0.75$ were carried out in order to determine the influence of α of the oil on the performance of the receivers containing a wire mesh. Hence, the models were also run with $\alpha = 600$ m^{-1} and with $\varphi = 0.75$. Plots (a) and (c) of Fig. 10 show that T_{max} are the same for the two light absorption coefficients. T_{mean} for oil with $\alpha = 2800$ m^{-1} is slightly less than that for oil with $\alpha = 600$ m^{-1}. A similar trend is also observed for T_{out}. However, the differences in T_{mean} and T_{out} for the two absorption coefficients are not significant.

Plot (b) of Fig. 10 for the VF receiver indicates that there is no significant difference in η_2 for the two cases of different absorption coefficients. This indicates that the wire mesh has a strong influence on η_2 as compared to α and this is because of its large thermal conductivity. η_3 of the VF receiver is greater for $\alpha =$ 2800 m^{-1} than for 600 m^{-1}. This implies that an increase in α of the oil, for the VF receiver with a wire mesh inserted, increases η_3. The overall influence of α on the VF receiver containing a wire mesh is shown in plot (b) and indicates that an increase in α increases its overall efficiency η_1.

Plot (d) of Fig. 10 for the VB receiver shows that there is no significant difference between η_1, η_2 and η_3 obtained either with $\alpha = 2800$ m^{-1} or with $\alpha = 600$ m^{-1}. A similar trend is observed for the temperatures. Thus, when the VB receiver contains a wire mesh, changes in α have little effect on its overall performance. The wire mesh has a dominant effect on the overall performance of the VB receiver. Thus, the use of a wire mesh also reduces the variation of the VB receiver performance that may be caused by changes in α.

The difference in the response of the two receivers to changes in α when they contain a wire mesh is because the VB receiver is largely made of aluminium while the VF receiver is largely made of glass.

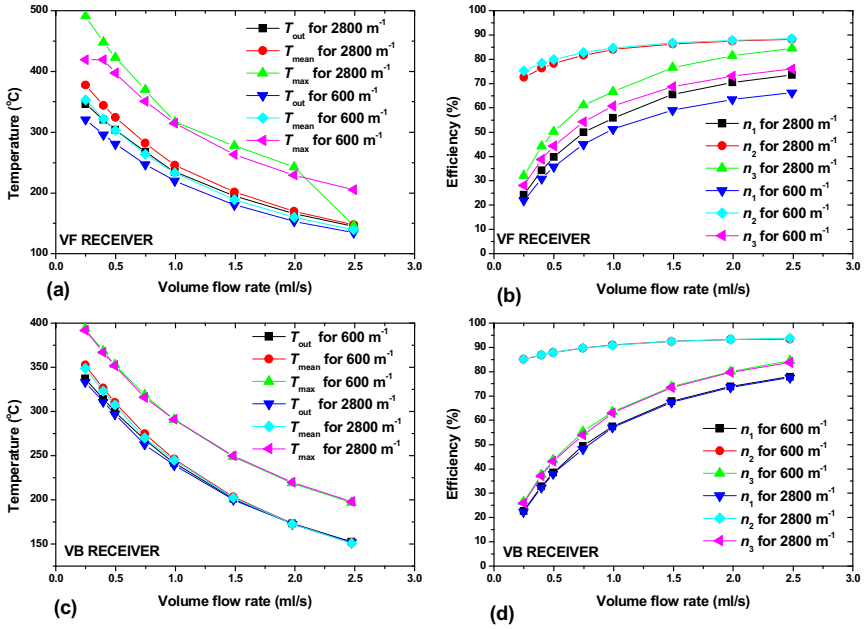

Fig. 10: The plots of the temperatures (a) and (c) and efficiencies (b) and (d) against the flow rate for the receivers that have φ = 0.75 and contain oil of α = 600 m^{-1} and α = 2800 m^{-1}.

4.2 Validation Process

The experimental results of the receivers were compared with those of their models in order to validate the models. We recall that the efficiency η_1 for each model is calculated by Eq. 1 in which P_{incident} is 730 W. Thus, in order to compare η_1 from the model and that from the experiment, η_1 from the model was recomputed with P_{incident} of 1500 W which is the approximate input solar power captured by the PDR. Fig. 11 shows a comparison of the receivers' efficiencies predicted by their models and the experimental efficiencies. Plots (a) and (c) of the figure show that the model efficiencies (for α = 2800 m^{-1}) are slightly lower than the experimental efficiencies. The reason for this is the difference in α of the oil that is used in the model and the actual α of Thermia B oil that is used in the experiment. In order to verify this, the experimental efficiencies were compared against the model efficiencies for the same receiver models containing oil of α = 600 m^{-1} and plots (b) and (d) of Fig. 11 show the result. The plots indicate that the experimental and model efficiencies are more comparable than shown in plots (a) and (c). This indicates that the receiver models having oil of α = 600 m^{-1} represent fairly the actual receivers. The receiver models having oil of α = 2800 m^{-1} represent efficiencies that would be obtained if oil of a higher absorption coefficient was used in the experimental evaluation of the receivers.

Fig. 12 shows the predicted efficiency (η_1) from the receiver models that have a wire mesh and that contain oil with different absorption coefficients together with the experimental η_1 when the receivers contain the wire mesh. In plots (a) and (b) where the VF receiver model contains oil with α = 2800 m^{-1} and 600 m^{-1} respectively, the predicted and the experimental η_1 are equal for all mass flow rates though the predicted η_1 is slightly reduced in plot (b). This is because of the dominant effect of the wire mesh which tends to override the effect of changes in α. Thus, the wire mesh has a dominant effect on the performance of the VF receiver than α of the oil. Hence, by inserting a wire mesh into the VF receiver the possibility of its performance changing due to changes in α of the oil are reduced.

Plots (c) and (d) of Fig. 12 show that the predicted η_1 from the model of the VB receiver that has a wire mesh and containing oil of α = 2800 m^{-1} or α = 600 m^{-1} is higher than the experimental efficiency when the VB receiver contains a wire mesh. The model efficiencies are both higher for the two α-values. This is because in the model, the wire mesh is evenly distributed throughout the oil zone and there is good contact between the wire mesh and the glass forming the aperture and the receiver walls while in the actual receiver, the mesh is not in contact with the glass at the receiver aperture. The other reason is that in the actual

receiver, there is poor contact between the receiver wall and the wire mesh and as such, heat transfer through conduction between the receiver walls and the wire mesh is not enhanced. This implies that when inserting the wire mesh into the receiver it must be done such that there is good contact between the wire mesh and both the receiver walls and the glass at the aperture.

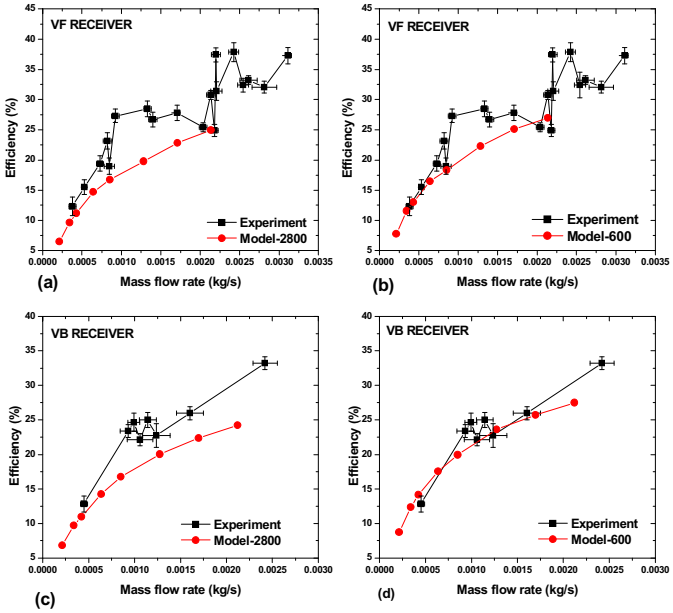

Fig. 11: A comparison of the efficiencies obtained from the experiments and the receiver models containing oil of $\alpha = 2800$ m^{-1} and $\alpha = 600$ m^{-1}.

The results show that in general, the receiver models with oil of α = 600 m^{-1} fairly represent the actual physical receivers and hence can be used to further optimise the performance of the receivers without the need to actually re-construct the receivers and carry out experimental work. In this way modelling the receiver would help towards reducing time and cost normally associated with carrying out experimental work. The use of a wire mesh has been observed to improve the performance of the receivers.

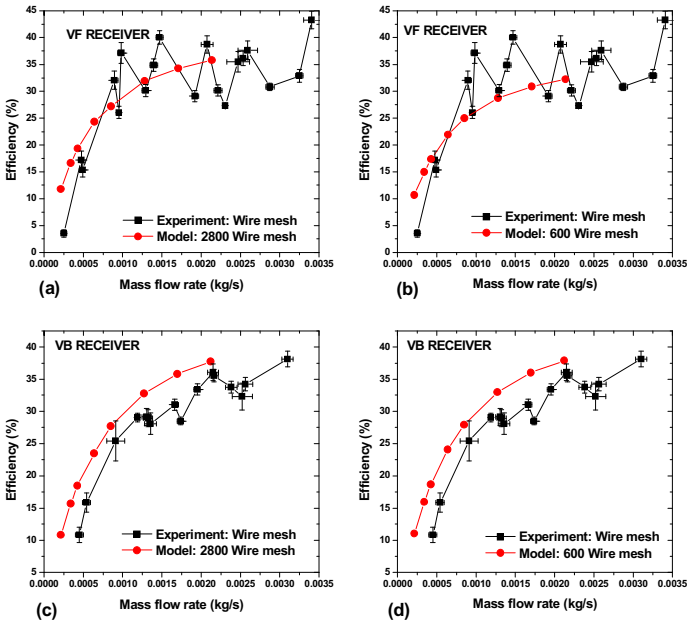

Fig. 12: A comparison of the experimental η_1 of the receivers containing a wire mesh and the receiver models containing a wire mesh ($\varphi = 0.75$) and containing oil of different α-values.

5. Conclusions

Two receivers were designed and optimised using CFD models. Based on the models, two prototypes were built and tested. The models were then validated with experimental data and the results are in fair comparison. Since the model results with oil of α = 600 m^{-1} and the experiments are comparable, it means that the experimental oil has a similar α-value. The models show that the wire mesh increases the receiver efficiency and reduces the maximum temperatures in the receivers. A wire mesh of $\varphi \approx 0.95$ is sufficient to improve the efficiency of the receivers while at the same time it reduces the pressure drop within the receivers.

Acknowledgements

The first author (JSPM) is grateful to the University of Malawi for granting a study leave and the DAAD for a studentship.

References

Comakli O., Bayramoglu M., Kaygusuz K., 1996. A thermodynamic model of a solar assisted heat pump system with energy storage. Solar Energy. 56, 485-492.

Hasuike H., Yoshizawa Y., Suzuki A., Tamaura Y., 2006. Study on design of molten salt solar receivers for beam-down solar concentrator. Solar Energy. 80, 1255-1262.

Kribus A., Zaibel R., Carey D., Segal A., Karni J., 1998. A solar-driven combined cycle power plant. Solar Energy. 62, 121-129.

Mawire A., McPherson M., van den Heetkamp R.R.J., Mlatho J.S.P., 2009. Simulated Performance of a storage materials for pebble bed thermal energy storage (TES) system. Applied Energy. 86, 1246-1252.

Meier A., Ganz J., Steinfeild A., 1996. Modeling of a novel high-temperature solar chemical reactor. Chemical Engineering Science. 51, 3181-3186.

Mlatho J.S.P., McPherson M., Mawire A., van den Heetkamp R.J.J., 2010. Determination of the spatial extent of the focal point of a parabolic dish reflector using a red laser diode. Renewable Energy. 35, 1982-1990.

Pitz-Paal R., Hoffschmidt B., Böhmer M., Becker M., 1997. Experimental and Nummerical evaluation of the performance and flow stability of different types of open volumetric absorbers under non-homogeneous irradiation. Solar Energy. 60, 135-150.

Reddy K.S., Satyanarayana G.V., 2008. Numerical study of porous finned receiver for solar parabolic trough concentrator. Engineering Applications of Computational Fluid Mechanics. 2, 172-184.

Shell., 2007. Shell Thermia oil B – High performance heat transfer fluid. Available: http://www.epc.shell.com/Docs/GPCDOC_X_cbe_24855_key_140002282412_1C93.pdf [accessed 05.05.2008].

Souza R.F., Alencar M.A.R.C., Meneghetti M.R., Hickmann M., 2006. Nonlinear optical properties of castor oil, XXIX ENFMC – Annals of optics. Available: http://www.sbf1.sbfisica.org.br/procs/2006/pdfs%20optics/non-linear%20optics/1227%20-1.pdf [accessed 01.09.2008].